Supporting Information

Atomistic insights into the layered microstructure and time-dependent stability of [BMIM][PF_6] confined within the meso-slit of carbon

Zhongyang Dai, Yajing You, Yudan Zhu*, Shanshan Wang, Wei Zhu, Xiaohua Lu

College of Chemical Engineering, State Key Laboratory of Materials-oriented Chemical Engineering, Nanjing Tech University, 30# Puzhu South Road, Nanjing 211816, P.R. China

*E-mail: ydzhu@njtech.edu.cn (Yudan Zhu)

Nonbonded force field parameter

[BMIM][PF_6] ionic liquids (ILs) are described by the refined force field of imidazolium-based ionic liquids developed by Liu *et al.*[1] This model was modified based on the AMBER force field, and the simulation results are in good agreement with experiment data, especially on the density, interaction energy, and diffusion constant.[1,2] The force field of graphene sheet was obtained from reference 3. The Lennard-Jones 12-6 (see Eq.1) and coulombic potential models (see Eq.2) were employed to describe the van der Waals (vdW) and electrostatic interactions, respectively. All detailed nonbonded parameters, including [BMIM][PF_6] and graphene, are listed in Table S1.

$$E_{vdW} = 4\varepsilon\left[\left(\frac{\sigma}{r}\right)^{12} - \left(\frac{\sigma}{r}\right)^{6}\right] \qquad (1)$$

$$E_{coul} = \frac{q_i q_j}{\varepsilon_r \varepsilon_o r} \qquad (2)$$

In Eq.1, ε and σ represent the energy parameter and size parameter of atoms. In Eq.2, q_i, q_j represent the charge of atom i and atom j, ε_r represents the relative dielectric constant of [BMIM][PF_6] ILs, while ε_o represents the dielectric constant of vaccum.

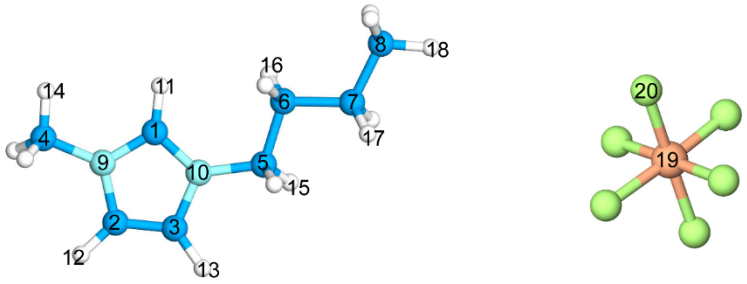

Table S1. The Lennard-Jones parameters and partial atomic charges used in this work.

id	atom type	ε (Kcal/mol)	σ (Å)	q (e)
1	C	0.086	3.4	-0.0055
2	C	0.086	3.4	-0.1426
3	C	0.086	3.4	-0.2183

4	C	0.1094	3.4	-0.0846
5	C	0.1094	3.4	-0.0153
6	C	0.1094	3.4	0.0107
7	C	0.1094	3.4	0.0309
8	C	0.1094	3.4	-0.0713
9	N	0.17	3.25	0.0596
10	N	0.17	3.25	0.0682
11	H	0.015	1.782	0.2258
12	H	0.015	2.511	0.2340
13	H	0.015	2.511	0.2633
14	H	0.0157	2.471	0.1085
15	H	0.0157	2.471	0.0796
16	H	0.0157	2.65	0.0204
17	H	0.0157	2.65	0.0157
18	H	0.0157	2.65	0.0294
19	P	0.2	3.742	0.7562
20	F	0.061	3.118	-0.2927
graphene	C	0.07	3.55	0.000

Table S2. Fitting parameters and the rotational relaxation time τ_r (ps) of imidazolium rings, butyl chains and anions in the different layer regions of graphene slit as well as the corresponding bulk values for comparison.

system		A	B	C	τ_a	τ_b	τ_c	τ_r
imidazolium ring (cation)	com-layer	0.69	0.15	0.16	1190.48	105.83	2.01	835.84
	sub-layer	0.31	0.40	0.29	320.17	46.54	1.99	118.08
	cen-layer	0.03	0.48	0.49	1346.74	93.65	5.99	92.46
	bulk	0.47	0.32	0.21	46.99	12.88	0.55	26.32
butyl chain (cation)	com-layer	0.62	0.26	0.12	4857.78	4622.89	23.42	4187.43
	sub-layer	0.70	0.19	0.11	710.19	107.04	1.79	516.75
	cen-layer	0.62	0.25	0.13	498.06	123.15	2.90	339.14
	bulk	0.07	0.79	0.14	339.74	118.59	2.59	117.14
anion	com-layer	0.12	0.64	0.24	0.08	0.46	1.56	0.69
	sub-layer	0.12	0.67	0.21	0.09	0.38	0.96	0.47
	cen-layer	0.11	0.70	0.19	0.08	0.39	1.01	0.47
	bulk	0.12	0.66	0.22	0.08	0.38	0.85	0.45

Table S3. Diffusion coefficients derived from the *x*-*y* parallel and *z* perpendicular MSD components of [BMIM] cations and [PF_6] anions in the different layered regions. (*D**, the self-diffusion coefficients of bulk cations and anions were approximately 2.88×10^{-11} and 1.82×10^{-11} m^2s^{-1}, respectively)

	$D_{x\text{-}y}$ (10^{-9} m^2s^{-1})		D_z (10^{-12} m^2s^{-1})	
	cation	anion	cation	anion
com-layer	2.97	2.97	0.25	0.10
sub-layer	2.97	2.98	1.50	1.00
cen-layer	2.98	2.97	10.5	3.50
bulk	*D**			

We constructed a larger graphene sheet with dimensions of 7.15×7.23 nm^2, and randomly inserted 394 pairs of [BMIM][PF_6] ILs in the 2.8 nm-wide slit. We compared the spatial distributions of cationic imidazolium rings and anions. As shown in Figure S1(a) and (b), the number density profiles obtained from the two models were identical. This result demonstrates that the graphene length used in our work is sufficient and reasonable.

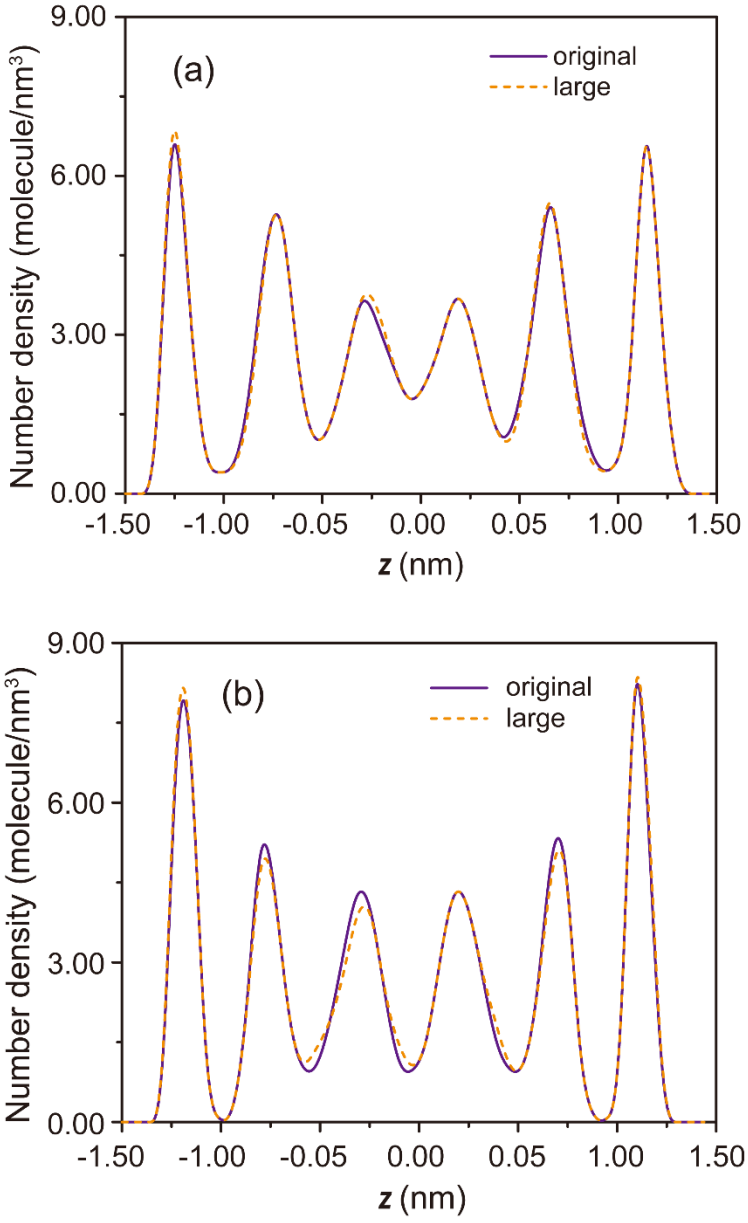

Figure S1. Number density profile along the *z*-axis of (a) imidazolium rings and anions using the 5.65×5.53 nm^2 graphene (original) and 7.15×7.23 nm^2 graphene (large).

To ensure that the image effect in the *z*-axis direction was eliminated, we performed another simulation, in which the periodic boundary condition was not used in the *z*-axis direction. The orientation distributions of the imidazolium ring using two different methods were compared. Figure S2(a), (b) and (c) showed the orientation distribution of the imidazolium ring in the com-, sub-, and cen-layer region, respectively. We found that the orientation distribution curves obtained from the two methods were identical. This phenomenon proves that a 5 nm vacuum on the upper and lower parts of the graphene sheet was sufficient to eliminate the image effects in the *z*-axis direction.

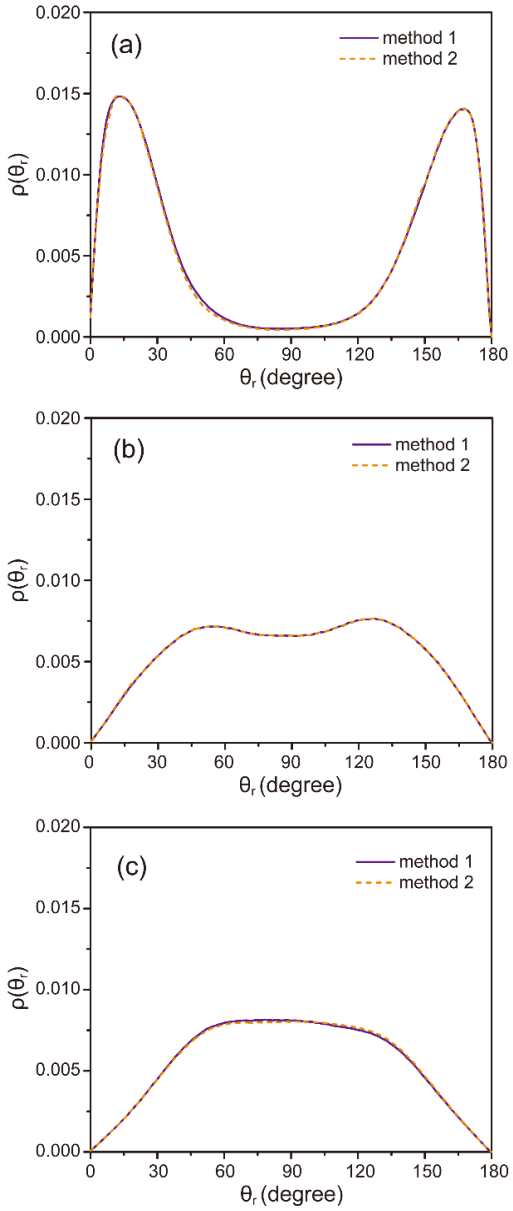

Figure S2. Orientation distribution of the imidazolium ring in the (a) com-, (b) sub-, and (c) cen-layer region using two different methods (method1: using periodic boundary condition in all directions and keeping a 5 nm vacuum on the upper and lower parts of the graphene sheet; method2: without periodic boundary condition in the *z*-axis direction).

Spatial distribution along the *z*-axis in the larger carbon slit

We performed two other simulations, in which the slit width was 4.8 and 6.8 nm, respectively. The density distribution of the imidazolium ring of [BMIM] cation in the three slits are shown in the Figure S3(b) and (c). We found that in the larger 4.8 and 6.8 nm carbon slits, the spatial distribution of the imidazolium ring along the *z*-axis direction exhibits two sharp peaks near the graphene, whereas no obvious density peak exits in the middle region, suggesting that the properties of imidazolium-based ILs in the middle region are close to the bulk counterpart. This phenomenon indicates that in larger pores, the carbon slit exerts its effect on the confined ILs in the com- and sub-layer regions. However, [BMIM][PF_6] ILs in the 2.8 nm meso-slit of carbon formed three distinctive layered regions, which are all different from its bulk counterpart.

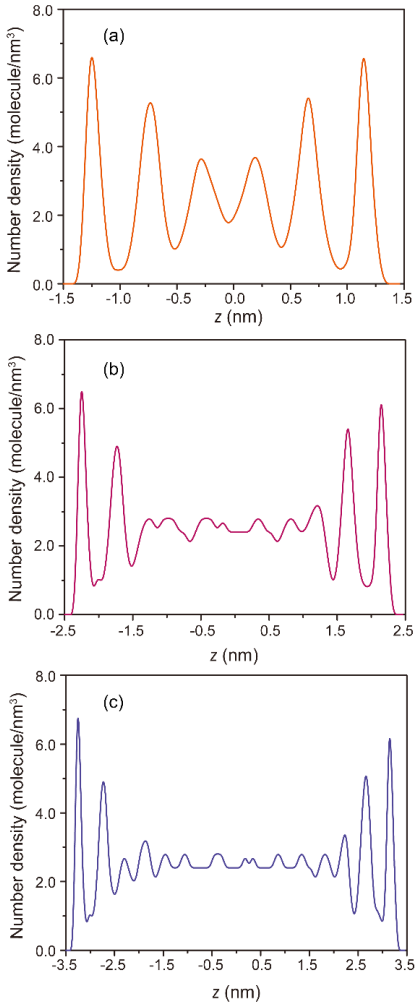

Figure S3. Number density profiles along the *z*-axis of the imidazolium ring inside the (a) 2.8, (b) 4.8, and (c) 6.8 nm carbon slits.

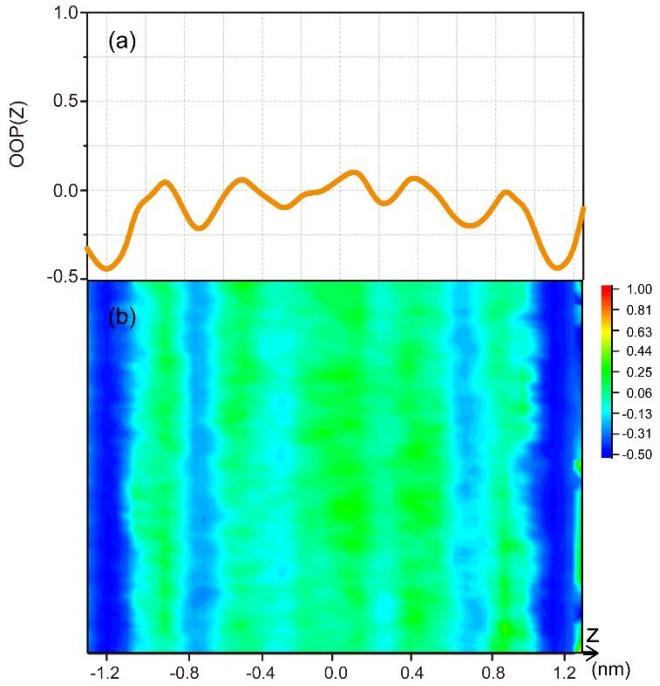

Figure S4. (a) Butyl chain OOP distribution along the *z*-axis. (b) Butyl chain OOP two-dimensional density distribution.

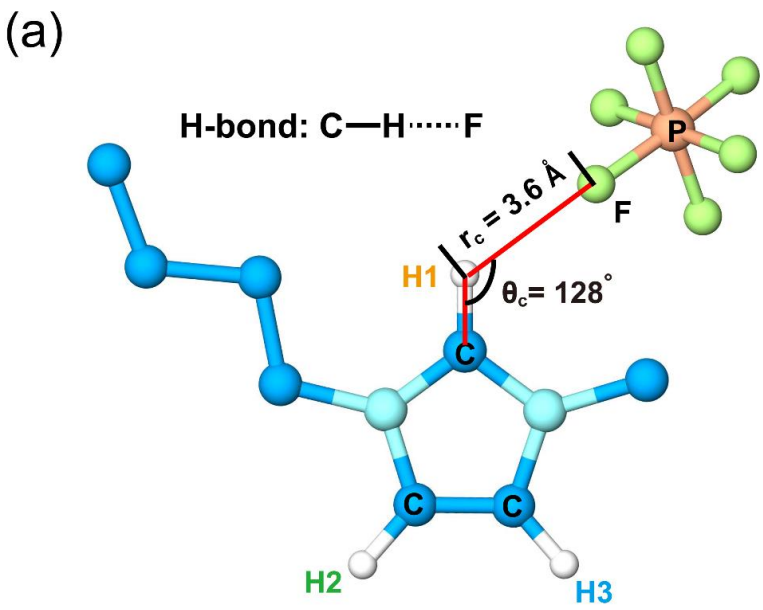
(a)
H-bond: C—H·····F
P
F
r_c = 3.6 Å
H1
θ_c= 128°
C
C
C
H2
H3

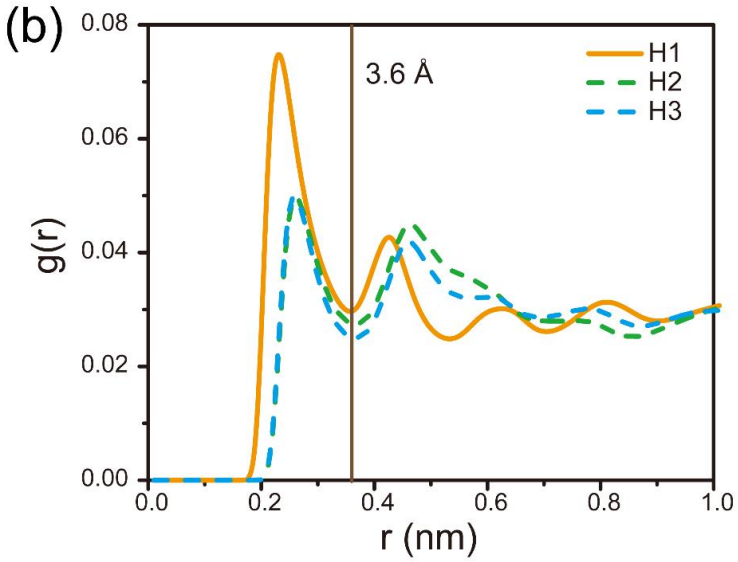
(b)
0.08
0.06
0.04
0.02
0.00
g(r)
3.6 Å
H1
H2
H3
0.0
0.2
0.4
0.6
0.8
1.0
r (nm)

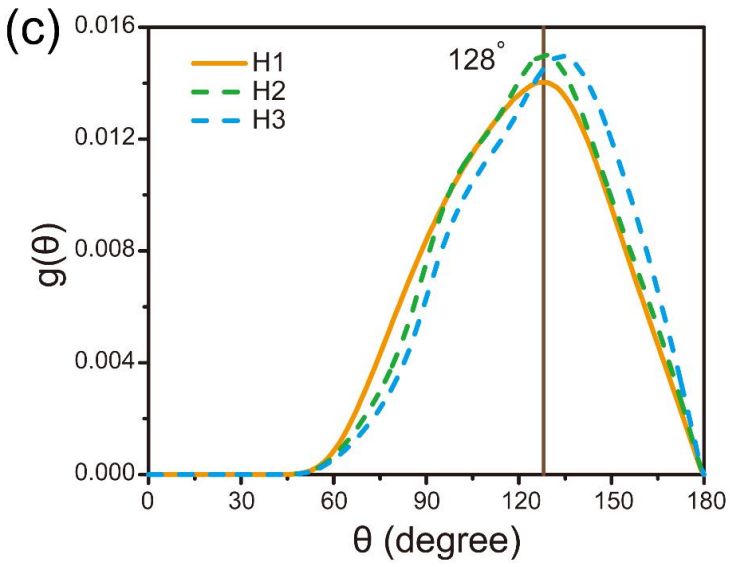
(c)
0.016
0.012
0.008
0.004
0.000
g(θ)
H1
H2
H3
128°
0
30
60
90
120
150
180
θ (degree)

Figure S5. (a) Schematics for the HB definition between [BMIM] cations and [PF_6] anions. Here, the distance and angle criteria are obtained according to (b) the RDF between the imidazolium H atoms and the F atoms of anion and (c) the corresponding angle distribution functions.

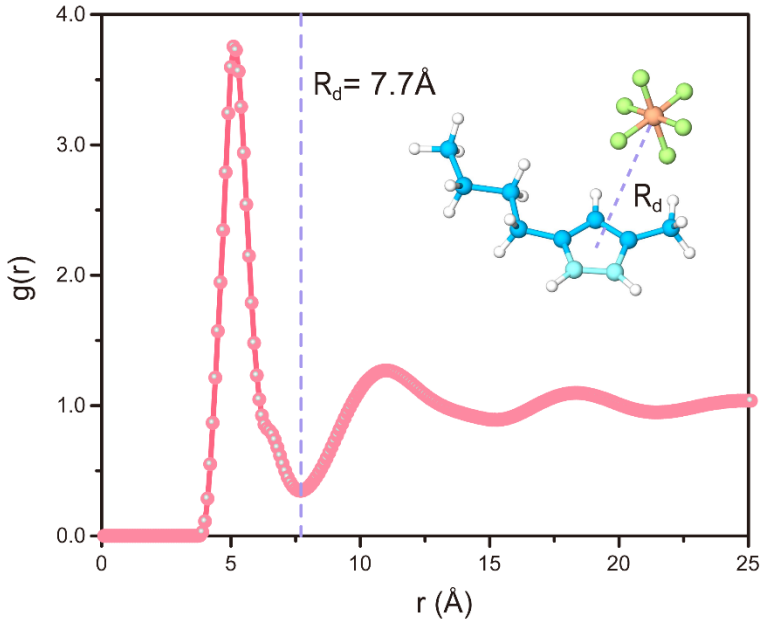

Figure S6. The radial distribution function (RDF) of the geometric centers between imidazolium rings and anions.

Translational motion of cations and anions

The mean square displacement (MSD) is calculated to evaluate the translational mobility of cation–anion pairs, which is defined as

$$\mathrm{MSD} = \frac{1}{N}\left\langle \sum_{i=1}^{N} \left| r_i\,(t) - r_i\,(0) \right|^2 \right\rangle \qquad (3)$$

where $r_i\,(t)$ denoted the coordinates of the i^{th} molecule at time t. The geometric center of cationic imidazolium rings and [PF_6] anions were chosen as the characteristic fragments of cation–anion pairs. Then, the MSD components in the direction of parallel (i.e., x-y plane) and perpendicular (i.e., z-axis) to the graphene for [BMIM][PF_6] ILs in the different layered regions were calculated, respectively.

Figure S7(a) exhibited the *x*-*y* parallel MSD components of cations and anions. We found that those curves almost coincided. This means that the *x*-*y* parallel translational mobilities of cations and anions in the different layered regions were identical. Figure S7(b) showed the *z* perpendicular MSD component of cations and anions. Generally, the slopes of *z* perpendicular MSD component curves were obviously less than those of *x*-*y* parallel MSD component curves. This phenomenon suggests that the translational mobility in the *z*-axis direction is significantly slower than that in the *x*-*y* plane for ILs confined in 2.8 nm meso-slit of carbon. As shown in Figure S7(b), we found that for [BMIM] cation (or [PF_6] anion) in the different layered regions, their slopes follow the sequence of cen-layer > sub-layer > com-layer. In the same layered region, the slope of cation curve is larger than that of the anion curve. This phenomenon indicates that the translational mobility of ions in the *z*-axis direction follows cen-layer > sub-layer > com-layer, and that in the same layered region, cationic translational motion is quicker than that of anions. The similar phenomenon has been found for imidazolium-based IL near the graphene.[4] We also calculated the MSD of bulk [BMIM] cations and [PF_6] anions, as shown in Figure S8. Using the Einstein relation,[5-6] the diffusion coefficients of cations and anions of different layered regions ($D_{x\text{-}y}$ and D_z) and the bulk ones (D^*) were calculated and listed in the Table S3. The self-diffusion coefficients of bulk cations and anions were approximately 2.88×10^{-11} and 1.82×10^{-11} m^2s^{-1}, respectively. The simulation results of bulk ILs are in the same magnitude with that reported in previous simulations.[1,4] In the Table S3, we also found that the *x*-*y* planed diffusion coefficients of the cations and anions in the meso-slit were obviously larger than their bulk self-diffusion coefficients. This phenomenon indicated that 2.8 nm meso-slit of carbon promoted the translational motion of [BMIM][PF_6] in the direction paralleled the graphene sheets.

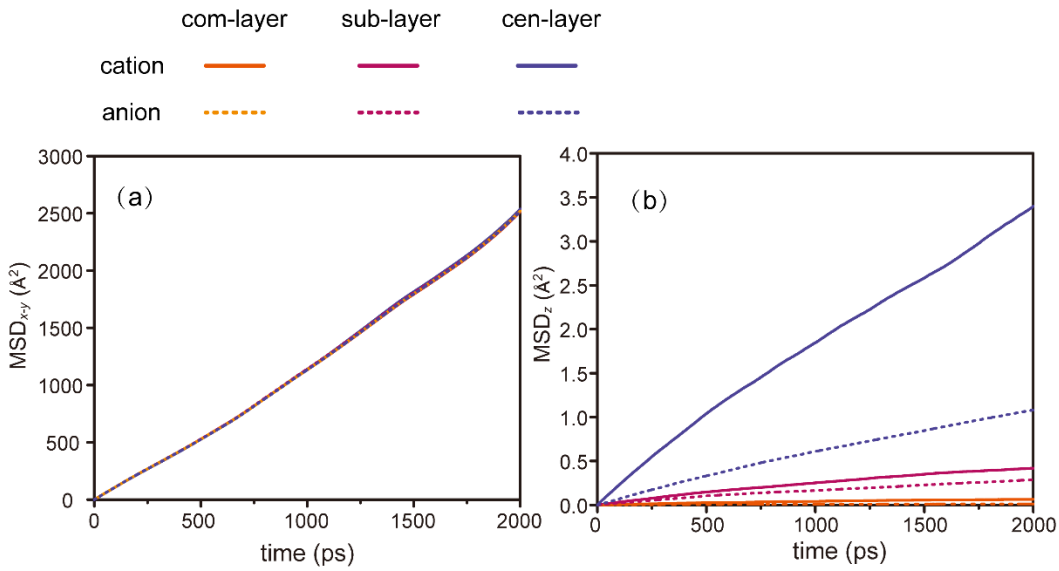

Figure S7. (a) *x*-*y* parallel and (b) *z* perpendicular MSD components of [BMIM] cations and [PF_6] anions in the different layered regions.

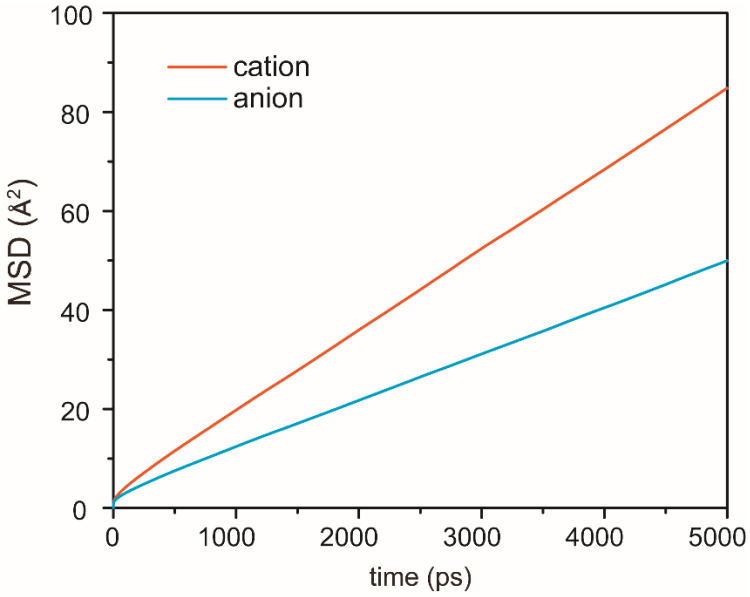

Figure S8. MSD curves of [BMIM] cations and [PF_6] anions in the bulk.

References:

(1) Liu, Z. P.; Huang, S. P.; Wang, W. C. A refined force field for molecular simulation of imidazolium-based ionic liquids. *J. Phys. Chem. B* **2004**, 108, 12978-12989.

(2) Dommert, F.; Schmidt, J.; Qiao, B.; Zhao, Y.; Krekeler, C.; Delle S. L.; Berger, R.; Holm, C. A comparative study of two classical force fields on statics and dynamics of $EMIMBF_4$ investigated via molecular dynamics simulations. *J. Chem. Phys.* **2008**, *129*, 224501-224511.

(3) Shao, Q.; Zhou, J.; Lu, L. H.; Lu, X. H.; Zhu, Y. D.; Jiang, S. Y. Anomalous hydration shell order of Na^+ and K^+ inside carbon nanotubes. *Nano Lett.* **2009**, *9*, 989-994.

(4) Wang, Y. L.; Lu, Z. U.; Laaksonen A. Heterogeneous dynamics of ionic liquids in confined films with varied film thickness. *Phys. Chem. Chem. Phys.* **2014**, 16, 20731-20740.

(5) Holden, D.; Jelfs, K. E.; Trewin, A.; Willock, D. J.; Haranczyk, M.; Cooper, A. I. Gas diffusion in a porous organic cage: analysis of dynamic pore connectivity using molecular dynamics simulations. *J. Phys. Chem. C* **2014**, 118(24): 12734-12743.

(6) Liu, Y.; Fu, J.; Wu, J. Excess-entropy scaling for gas diffusivity in nanoporous materials. *Langmuir* **2013**, 29(42): 12997-13002.